Microscopic single molecule dynamics suggest underlying physical properties of the silencing foci

Susmita Sridar [1 †] ✉, **Mathias Spliid Heltberg** [2 †] ✉, **Christian Michelsen** [2 †], **Judith Mine Hattab** [1], **Angela Taddei** [1]

[1]Institut Curie, PSL University, Sorbonne Universite, CNRS, Nuclear Dynamics, Paris, France; [2]Niels Bohr Institute, University of Copenhagen

✉ **For correspondence:** mathias.heltberg@nbi.ku.dk (MH)

[†]Authors contributed equally.

Present address: Niels Bohr Institute, University of Copenhagen, Blegdamsvej 17, 2100 Copenhagen, Denmark

Data availability: Data availability is available on Zenodo or the Github repository.

Funding: This work was supported by XXX Foundation. The funders had no role in the decision to publish.

Competing interests: The author declare no competing interests.

Abstract

In order to obtain fine-tuned regulation of protein production while maintaining cell integrity, it is of fundamental importance to living organisms to express a specific subset of the genes abailable in the genome. One way to achieve this is through the formation of subcompartments in the nucleus, known as foci, that can form at various locations on the DNA fibers and repress the transcriptional activity of all genes covered. In this work we investigate the physical nature of such foci, by applying single molecule microscopy in living cells. Here we study the motion of the protein SIR3. By combining various statistical methods, and combining a frequentist with a bayesian approach, we extract the diffusion properties for motion in a repair foci. In order to obtain useful information based on this, we derive similar measures for the foci itself, the motion of SIR3 outside the foci and other mutants of the cell. We reveal that the behaviour inside a repair foci is highly immobile and we compare this to theoretical expressions. Based on this we hypothesize that the repair foci is probably not a result of a second order liquid-liquid phase separation but rather a so-called Polymer Bridgng Model with numerous binding sites.

1 | INTRODUCTION

Understanding the physical principles of how cells can express and silence specic regions of the genome presents one of the most fundamental challenges in biology. As a model to study this, budding yeast chromosomes is a strong candidate, since it has very few repetitive sequences outside of the rDNA compared to other eucaryotes that contain centromeric hetero-chromatin. When haploid cells grow at their maximal rate, one characteristic aspect is that 32 telomeres accumulate at the nuclear envelope allowing them to form ≈3–5 foci. The sizes of these are in the order of a few hundreds of nanometer and therefore below the diffraction limit of conventional epifluorescence microscopes.

Inside such foci, the silent regulatory factors Sir2, Sir3 and Sir4 concentrate into the form of the SIR complex (Palladino et al., 1993). These are therefore termed silencing foci, since they can repress the expression of the underlying genes through interaction with the telomeric protein Rap1, and thereby spread on chromatin and potentially forming a compact chromatin structure. Studies in vitro has revealed that this complex associates with nucleosome in a 1:2:1 stochiometry and can significantly compact chromatin (Swygert et al., 2018).

The sequestration of SIR proteins from silent chromatin favor the subtelomeric repression and the position of telomeres inside these foci favors faithful recombination events upon double strand break (Batté et al., 2017). Furthermore, it also prevents the binding of the SIRs at specific groups of promoters in the genome (Maillet et al., 1996; Marcand et al., 1996; Taddei et al., 2009).

In the foci, the telomere composition is not fixed, however telomeres show preferential attachment to other telomeres coupled to chromosome arms of approximately equal length (Therizols et al., 2010; Schober et al., 2008; Duan et al., 2010). This process of telomeres grouping in a limited number of foci requires Sir3 association to telomeres but is independent of heterochromatin formation (Ruault et al., 2011) and these foci has been revealed to fuse into bigger foci or hyperclusters when SIR3 is overexpressed, suggesting a regulatory role on telomere clustering for SIR3 (Ruault et al., 2011).

In this work we investigate the physical mechanism of the formation of silencing foci. In particular we use using Single Particle Tracking (SPT) and Photo Activable Localization Microscopy (PALM) in

Saccharomyces cerevisiae cells in order to obtain precise information obout the dynamics of single particles in the heterogenous environment. In this, SPT is a powerful technique that makes the microscopic steps taken by the molecules observable, by taking "live" recordings of individual molecules in a cell at high temporal and spatial resolution (50 Hz, 30 nm) (Dolgin, 2019; Manley et al., 2008; Oswald et al., 2014). Based on this in vivo movement, SPT allows for grouping specific proteins into subpopulations defined by the measured diffusion coefficients. From this it is possible to quantify the motion of each subpopulation and thereby estimating the residence times in different parts of the nucleus, allowing us to estimate the free-energy of the system. To assist the SPT measurements, PALM can establish a density maps of the molecules of interest by their position at 30 nm resolution.

Using these methods we have assessed the dynamics of SIR3 cells with silencing foci. We find that inside the silencing foci, SIR3 moves significantly slower and we relate this to the motion of the the whole focus itself. This allow us to identify the diffusion properties of both free telomeres, and telomeres inside a focus. Next we apply, Sir4 deprived mutants and observe that the foci has disappeared, allowing us to extract the free diffusion coefficient of SIR3. Finally we use this to extract the free energy of the molecules inside the repair foci, and we compare this to the theoretical prediction, assuming that the repair foci belongs to the Polymer-Bridging model. Here we find a good agreement, thus suggesting that the physical nature of these foci is really a dense collection of multiple binding sites that suppress the movement of molecules while enhancing their concentration is the formed region.

2 | METHODS & MATERIALS

2.1 | Diffusion model

For each of the different types of data (XXX), we load in the cells and group them by cell number and ID. For each group we compute the distance Δr between the subsequent observations $\vec{x}_i$:

$$\Delta r_i = \|\vec{x}_{i+1} - \vec{x}_i\|. \tag{1}$$

E.g., for Wild Type 1, we find 914 groups across 43 different cells, leading to a total of $N = 10.025$ distances. We model the diffusion distances with a Rayleigh likelihood, where the Rayleigh distri-

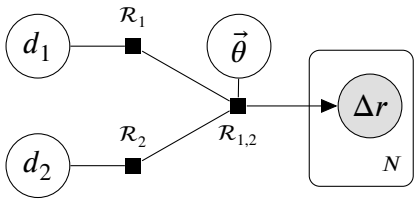

Figure 1. A graphical representation of the Bayesian model case of two diffusion components using the directed factor graph notation (Dietz, 2022). Here d_1 is the diffusion coefficient, $\mathcal{R}_1$ is the d-parameterized Rayleigh distribution and $\mathcal{R}_{1,2}$ is the mixture model of the Rayleigh distributions with a θ prior.

---

bution is given by:

$$\text{Rayleigh}(r;\sigma) = \frac{r}{\sigma^2} e^{-r^2/(2\sigma^2)}, \quad x > 0. \tag{2}$$

In this study, we parameterize the Rayleigh distribution in terms of the diffusion coefficient d, which is related to the scale parameter σ in eq. (2), through the XXX parameter, τ:

$$\sigma = \sqrt{2d\tau}, \tag{3}$$

with $\tau = 0.02$ in the current study. In the simplest form, where we assume only a single diffusion coefficient, d, the Bayesian model for this process is:

$$\begin{aligned}
&[d \text{ prior}] && d \sim \text{Exponential}(0.1) \\
&[\text{transformation}] && \sigma = \sqrt{2d\tau} \\
&[\text{likelihood}] && \Delta r_i \sim \text{Rayleigh}(\sigma).
\end{aligned} \tag{4}$$

A more realistic diffusion model include more than a single diffusion coefficient. Figure 1 shows this for the two-component case in directed factor graph notation (Dietz, 2022). In particular, the figure shows the combination of the $K = 2$ diffusion coefficients d_k through a mixture model $\mathcal{R}_{1,2}$ of the two d-parameterized Rayleigh distributions $\mathcal{R}_k$ with a v-prior. We model each of the distances as independent, indicated by the N-replications plate. In equations, the figure is similar to:

$$\begin{aligned}
&[d_1 \text{ prior}] && d_1 \sim \text{Exponential}(0.1) \\
&[d_2 \text{ prior (ordered)}] && d_2 \sim \text{Exponential}(0.1), \quad d_1 < d_2 \\
&[\vec{\theta} \text{ prior}] && \theta_1 \sim \text{Uniform}(0,1), \quad \vec{\theta} = \left[\theta_1, 1-\theta_1\right] \\
&[\text{mixture model}] && \mathcal{R}_{1,2}(d_1, d_2, \vec{\theta}) = \text{MixtureModel}\left(\left[\mathcal{R}(d_1), \mathcal{R}(d_2)\right], \vec{\theta}\right) \\
&[\text{likelihood}] && \Delta r_i \sim \mathcal{R}_{1,2}(d_1, d_2, \vec{\theta}).
\end{aligned} \tag{5}$$

2.2 | Model comparison

We can generalize the $K = 2$ diffusion model to higher values of K by having $d_1, \ldots, d_K$ ordered[1] diffusion coefficients and letting the mixture model's $\bar{\theta}$-prior be a random variable from a flat Dirichlet distribution (such that $\sum_k \theta_k = 1$). We find that including up to three diffusion coefficients yields appropriate results. To compare the three models of different complexity, we compute the Widely Applicable Information Criterion (WAIC) (Watanabe, 2010) which is a generalized version of the Akaike information criterion (AIC) useful for Bayesian model comparison (Gelman, Hwang, and Vehtari, 2014). In short, the WAIC is an approximation of the out-of-sample performance of the model and consists of two terms, the log-pointwise-predictive-density, lppd, and the effective number of parameters p_{WAIC}:

$$\text{WAIC} = -2\left(\text{lppd} - p_{\text{WAIC}}\right). \tag{6}$$

The lppd is the Bayesian version of the accuracy of the model and p_{WAIC} is a penalty term related to the risk of over-fitting; complex models (usually) have higher values of p_{WAIC} than simple models, (McElreath, 2020). The minus 2 factor is just a scaling included for historical reasons leading to low WAICs being better. Given two models, A and B, we compute both the individual WAIC values, W_A and W_B, their standard deviations, σ_{W_A} and σ_{W_B}, their difference, $\Delta_{A,B}$, and the standard error of their difference, $\sigma_{\Delta_{A,B}}$.

2.3 | Implementation

The data analysis has been carried out in Julia (Bezanson et al., 2017) and the Bayesian models are computed using the Turing.jl package (Ge, Xu, and Ghahramani, 2018). We use Hamiltonian Monte Carlo sampling (Betancourt, 2018) with the NUTS algorithm (Hoffman and Gelman, 2011). In particular, each Bayesian model have been run with 4 chains, each chain 1000 iterations long after discarding the initial 1000 samples ("warm up").

3 | RESULTS

3.1 | Two diffusive populations identified at for SIR3 mobility in WT

We started out by using SPT to investigate the mobility of individual SIR3 proteins in vivo in WT cells. To obtain this imaging of SIR3 without altering its normal expression level, we constructed a line of haploid cells that express the endogenous SIR3 fused to Halo (Figure 2A and Materials

[1] ordered such that $d_1 < d_k < d_K$ to prevent the classical label-switching problem in the case of mixture models (McLachlan and Peel, 2004)

and methods). Before we visualized this on a PALM microscope (see Materials and methods), we incubated the exponentially growing cells with fluorescent and fluorogenic JF647. This is a dye that emits light when it is bound to Halo. We then used a low concentration of JF647 in order to obtain visible individual molecules (Ranjan et al., 2020; Figure 1B). With this setup, the SIR3-Halo bound to JF647 (SIR3-Halo/JF647) were visualized at 20 ms time intervals (50 Hz) in 2-dimensions during 1000 frames until all signal had decayed. A typical individual cell is shown in Figure 2B and the tracking of the individual molecules is visualised in Figure 2C and based on these we moved on to calculate the density and displacement maps of the SIR3 molecules. Here it should be noted that the tracking of SIR3 is performed in 2-dimensions and the molecules are observable as long as are inside the focal plan which is the z-section of about 400 nm (Figure 2D). After measuring all the traces, we computed the Probability Density Function for the trace lengths, and here we found that while the shortest traces seemed to follow an exponential decay, there was a tail with some very long traces (Figure 2E). Here it is important to note that the half-life time of JF6467 is approximately 2 seconds, meaning that the short traces are due to molecules moving out of the observable z-section and not the photo bleaching of the JF647 dyes.

We aimed to estimate the effective diffusion coefficient of SIR3 in the WT environment, and therefore we computed the displacement for all points in each trace separately, and grouped these into the displacement histogram (Hansen et al., 2018; Klein et al., 2019; Stracy and Kapanidis, 2017). In this way we could test the naive hypothesis that SIR3 molecules simply exhibit a single diffusive motion. We therefore fit the displacement histograms to a Rayleigh distribution (a one parameter fit), and use the resulting fit quality to determine if this hypothesis is sufficient to describe the obtained data. By using Maximum-likelihood minimisation, we extract the most likely value for the diffusion coefficient and based on this we use the Kolmogorov-Smirnoff (KS) test, obtaining a p-value of $p = 0.0001$, indicating that more complex motion takes place. To take into account that the molecules can diffuse inside the silencing foci and outside these, we introduce two subpopulations characterized by distinct diffusion coefficients (see Materials and methods). By analysing individual cells, we observe that single traces can be very long in a small region of space, indicating a lower diffusion coefficient (Figure 2F). By fitting the displacement histogram with the two-population fit, we reveal that this leads to a good agreement. We further introduce a third population of diffusion coefficients, but obtain similar quality of the fit arguing that two diffusion coefficients is sufficient to explain the motion of the data (Figure 2G).

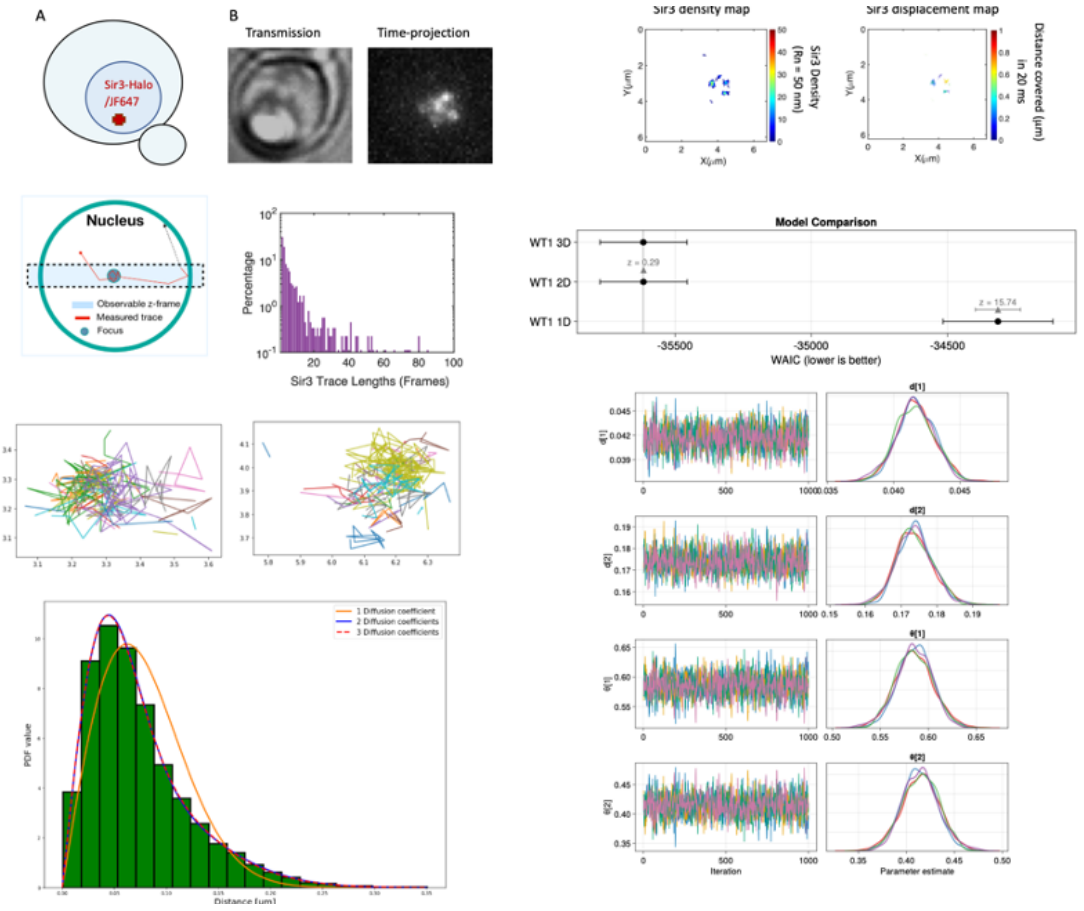

Figure 2. Mobility of Sir3 inside foci in WT cells.

Based on this we conclude that SIR3 in WT seem to have a motion defined by two distinct populations, significantly different from each other. While one of these populations has a very small diffusion coefficient, representing the motion inside the focus, the other seem to be slow compared to free molecules (compare to the free RAD52 for instance in Miné-Hattab et al., 2022). Therefore we hypothesise that this could be related to motion of SIR3 molecules attached to single telomeres, that are not part of the foci and therefore has higher mobility. In order to test this hypothesis, we tried to remove the existing foci and obtain the motion in this environment.

3.2 | Increased mobility of SIR3 in SIR2D-4D mutants

From the theory of silencing foci, it is well established that the proteins SIR2D and SIR4D should be present in order for the foci to assemble. Therefore, we hypothesised that by deleting these two related genes and thereby removing the availability of SIR2D and SIR4D, the silencing foci should not be able to form (Figure 3A). We succeeded in doing this, and observed that the motion of SIR3

seemed less dense at specific locations compared to the motion of WT (Figure 3B, compare to Figure 2B). Furthermore, we also noted that the traces seemed to be shorter and no traces were as long as the ones we observed in the WT conditions (Figure 3B). Therefore again computed the displacement histogram and used similar methods as described in Figure 2G to extract the diffusion coefficients. Again, we found that one diffusion coefficient could not explain the motion of SIR3, but two- and three subpopulations did indeed fit the data sufficiently well. Even though the three-diffusion coefficient fit did lead to a slight improvement in the fit, the two-population fitted the data very well (Figure 3C). This was further confirmed by turning to the Bayesian analysis, where we obtain a well-defined and unimodal distributions for each of the fitting parameters in the two-population fit (Figure 3D). By comparing the related WAIC scores, we also found that the three-population fit leads to a 1.28 σ increase in the fit quality, but since this is within statistical uncertainty, we conclude that the two-population fit has the most explanatory power of the observed data. By inspecting the diffusion coefficients here we note a very interesting aspect: While the slow diffusion coefficient, found in the WT motion, has disappeared in the SIR2D-4D mutant, the high diffusion coefficient for the WT is also identified in the motion of SIR3 in the SIR2D-4D mutant, but that a new faster population also has emerged. This supports our hypothesis that the slow observed diffusion coefficient in the WT is a result of the motion inside the foci, but that the fast diffusion coefficient does not represent freely diffusing molecules, but rather molecules attached the the semi-mobile telomeres. This also means that effectively all SIR3 molecules are bound in the WT suggesting a high number of binding sites and a high binding rate of these sites.

To further support these claims, we constructed a SIR2D mutant, that was deprived of SIR2 but still had SIR4 (Figure 3E). Here we again found a well distributed map of SIR 3 (Figure 3F), and by computing the displacement histogram we revealed that approximately the same diffusion coefficients existed in this mutant (Figure 3G – compare to Figure 3C). Here is seemed that the two-population fit differed slightly more from the three-population fit than the double mutant. To compare the quality of all hypotheses we again turned to the Bayesian analysis, where we could again find that all parameters in the two-population fit where smoothly, unmorally distributed, and while the three population fit had slightly better predictive power it was still only 1.78 σ and therefore within statistical uncertainty (Figure 3H).

Based on this, we conclude that by depriving the cell of SIR2 (and SIR4), the foci disappears and the mobility of SIR3 is increased and is described by two populations: A slow population repre-

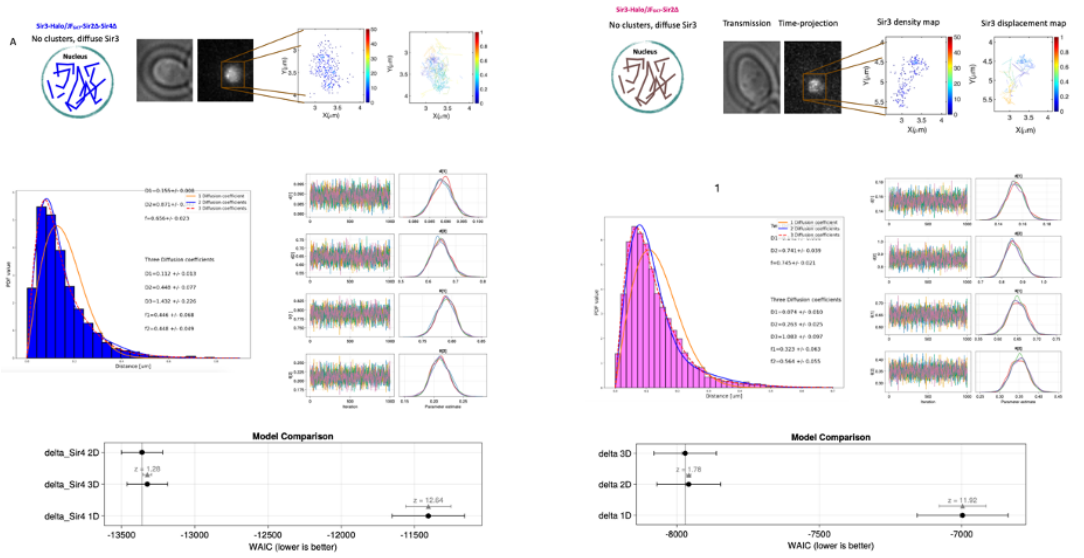

Figure 3. Mobility of Sir3 inside foci in mutant strains.

senting the bound molecules to single telomeres and a fast population representing the free SIR3 molecules. To understand the nature of the actual foci, we needed to understand the mobility of SIR3 inside the foci better. Therefore, we investigated the movement of the foci itself.

3.3 | Mobility of silencing foci is comparable to the motion of SIR3 inside the foci

Our aim was now to extract the motion of the foci as a single structure and compare this to the motion of the single molecules. In order to obtain this, we used high photo-activation illumination to simultaneously activate all SIR3-mMaple and image the silencing foci as a single entities. Here we are aware that the observed movement should now be dominated by the focus, but since the binding of single SIR3 molecules to the single telomeres, we should be aware that this could also be observed in the data (Figure 4A). We extracted the traces of these whole-mobility structures, and we obtained some confined slowly diffusing traces (blue part in Figure 4B) but also many faster moving traces (multiple colours in Figure 4B). By eye, this does suggest that some movement takes place as a well-defined structure (a silencing-focus) while other motion might be due to the more mobile single telomeres. To test this, we now generated the displacement histograms for the entities, and extracted the diffusion coefficients (Figure 4C). In order to compare the hypotheses of the subpopulations, we directly applied the bayesian analysis and while the two-parameter fit did again lead to well-defined parameters, the three-population fit did lead to a better fit (6.08 σ). We

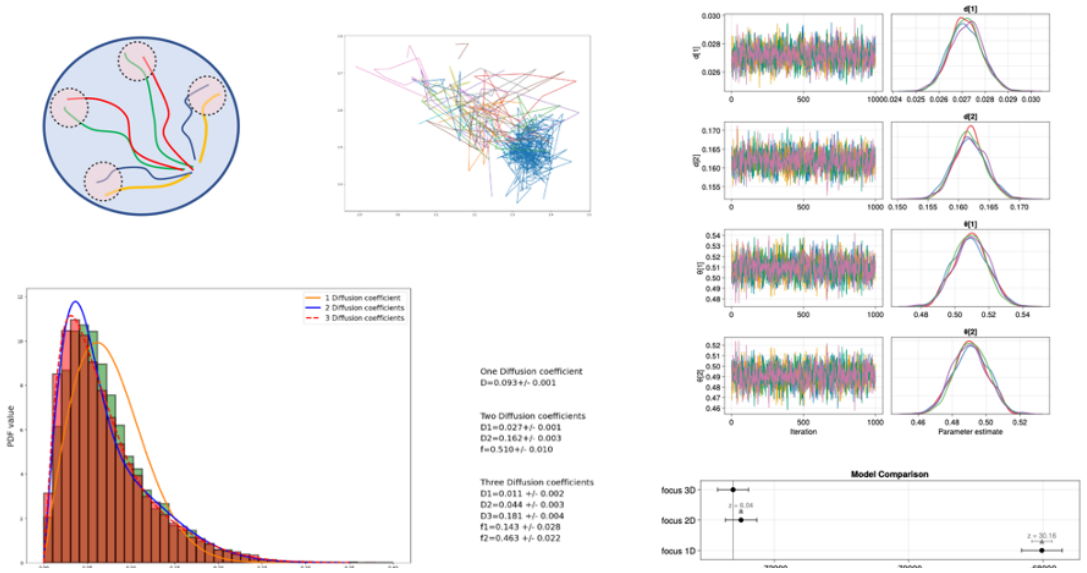

Figure 4. Individual Sir3 vs. whole focus.

note however that in both fits, the fast part of the population does match the diffusion coefficient of the single telomeres observed for single molecule SIR3 in both WT and SIR2D-SIR4D mutants. Now focusing on the slow part of the diffusion coefficients, we note that these match the extracted diffusion coefficients we found for the single molecule movement of SIR3. However to obtain a better understanding for the similarities of these, and in particular in order to extract the experimental noise levels in the measurements since these might differ significantly for the measurements of the entire focus and and measurements of the single SIR3, we moved on to measure the mean squared distance (MSD) and use these to extract the actual diffusion coefficients.

3.4 | Diffusion of SIR3 inside the silencing focus match the predicted movement of a Polymer Bridging Model

Our aim was now to extract the motion of the foci as a single structure and compare this to the motion of the single molecules. In order to obtain this, we used the previously derived theoretical result that connects the diffusion coefficient inside the foci structures to the free energy of these (Heltberg et al., 2021). Here the exact diffusion coefficient is extremely important and the result we obtained in section two is affected by the experimental noise level and this has a significant impact since the diffusion coefficient is so low. In order to separate these we used the method of Mean-Square Distances (MSD). Here we take the slow part of the population in the WT data, and for traces belonging to this family of diffusion coefficients we generate the mean square distances. Finally,

we fit the three first datapoints to a straight line, and use the slope as the diffusion coefficient whereas the intersection is a parameter determined by the experimental noise level. In order to obtain the free energy, we compare the fraction of traces belonging to the slow population, relative to the fast part of the population (See Miné-Hattab et al., 2022 for similar application). In this we take the size of the observable frame compared to the overall size of the cell nucleus into account, as well as we estimate an average of four foci on average. With this we obtain a relation between the free energy and the diffusion coefficient. We know that in a polymer bridging model this should scale as:

$$U = k_{\mathrm{BT}} \ln\left(\frac{D_{\mathrm{inside}} - D_{\mathrm{focus}}}{D_{\mathrm{outside}} - D_{\mathrm{focus}}}\right). \tag{7}$$

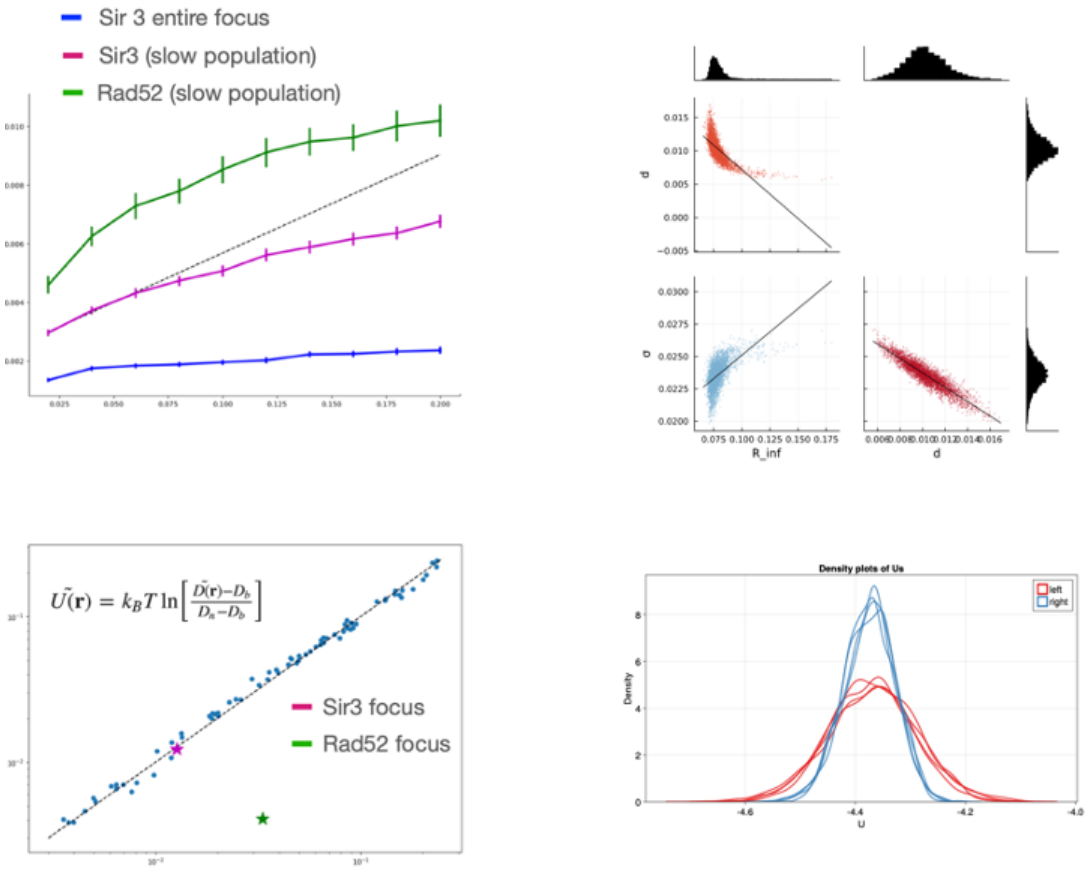

Figure 5. Free energy and diffusion relation. Relation to Rad52.

Here we assume that the diffusion coefficient of the focus is similar to the diffusion coefficient of the binding sites that would diffuse in a bridging model. We then used the simulation results of Heltberg et al., 2021, to show that in the simulations this type of structure always yield this relation and we showed the result of the relation in the repair foci that is markedly off this line (Figure 5B).

Finally we plotted the result for the silencing foci for the values obtained in this study and here we obtained a remarkable agreement. To further validate these results we used the Bayesian approach, where we tested the mutual correlation of the parameters investigated in the MSD curve (Figure 5C). Next we used this method to extract the free energy from the populations and compare this to the free energy estimate based on the extracted diffusion coefficients (Figure 5D). These were completely comparable, which further strengthens the conclusion that the motion inside the silencing foci is really comparable to what would be theoretically expected in the polymer bridging model.

4 | DISCUSSION

The two leading hypotheses for describing the nature of nuclear foci is the polymer bridging model and the liquid droplet model. In this work we have used the data obtained from SPT experiments to investigate the underlying nature of the silencing foci, experienced by the motion of SIR3. We find that the behaviour is comparable with the theoretical expectations of the polymer bridging model and this work therefore strengthens the hypothesis that these structures are indeed a dense collection of binding sites.

From a theoretical perspective, it is noteworthy that the method we apply here cannot directly falsify the hypothesis of a liquid structure, but rather it fails to disprove the hypothesis of a polymer bridging structure. We use a statistical mechanics formulation, derived a mean field, for the PBM. This shares the same functional form as the LPM in the sense that the diffusion coefficient follow a step function with one value inside the focus and another value outside. However for the PBM we have an additional constraint that precisely links the concentration of proteins and their relative diffusion inside the focus: the more time spent inside the focus, the slower the effective diffusion. In this sense, if the diffusion coefficient is higher than some value (To the right of the diagonal in Figure 4A), then this would typically represent a liquid droplet where diffusion can be faster.

From a functional perspective, it is also interesting to consider the role of a polymer bridging model, compared to a liquid model. The simplest form of a silencing foci, would simply keep away the transcription factors and activators. We have previously shown (Heltberg et al., 2021) that the existence of a polymer bridging model, would typically increase the first passage time to find a target, whereas a liquid model could greatly enhance this. Therefore it is a tempting hypothesis,

that foci formed with the aim of slowing down rates would be of a polymer bridging model, whereas the foci with the aim of increasing rates (for instance in the repair foci) could be liquid droplets. On a more general point, foci are formed inside the nucleus for various reasons with different roles, and it is clear that they can remain stable very different timescales. Here it is interesting that repair foci are maintained for relative short periods (timescale of hours) and they have the ability to quickly dissolve as long-term stability is not so important. On the other hand, gene expression foci can be very stable (Hnisz et al., 2017; Bing et al., 2020), and this could be explained by the hypothesis that these would typically be polymer bridging structures.

4.1 | Acknowledgment

Acknowledgements here

4.2 | Data availability

Source code is hosted at GitHub: https://github.com/ChristianMichelsen/diffusion.

REFERENCES

Batté, Amandine et al. (2017). "Recombination at subtelomeres is regulated by physical distance, double-strand break resection and chromatin status". eng. In: *The EMBO journal* 36.17, pp. 2609–2625. ISSN: 1460-2075. DOI: 10.15252/embj.201796631.

Betancourt, Michael (2018). "A Conceptual Introduction to Hamiltonian Monte Carlo". In: *arXiv:1701.02434 [stat]*. arXiv: 1701.02434.

Bezanson, Jeff et al. (2017). "Julia: A fresh approach to numerical computing". In: *SIAM review* 59.1. Publisher: SIAM, pp. 65–98. URL: https://julialang.org/.

Bing, X. Y. et al. (2020). "SnapShot: The Regulatory Genome". en. In: *Cell* 182.6, 1674–1674.e1. ISSN: 0092-8674. DOI: 10.1016/j.cell.2020.07.041. URL: https://www.sciencedirect.com/science/article/pii/S0092867420309491 (visited on 2022).

Dietz, Laura (2022). "Directed factor graph notation for generative models". In.

Dolgin, Elie (2019). "The sounds of science: biochemistry and the cosmos inspire new music". en. In: *Nature* 569.7755. Bandiera_abtest: a Cg_type: Books And Arts Number: 7755 Publisher: Nature Publishing Group Subject_term: Arts, Culture, pp. 190–191. DOI: 10.1038/d41586-019-01422-0. URL: https://www.nature.com/articles/d41586-019-01422-0 (visited on 2022).

Duan, Zhijun et al. (2010). "A three-dimensional model of the yeast genome". eng. In: *Nature* 465.7296, pp. 363–367. ISSN: 1476-4687. DOI: 10.1038/nature08973.

Ge, Hong, Kai Xu, and Zoubin Ghahramani (2018). "Turing: A Language for Flexible Probabilistic Inference". en. In: *Proceedings of the Twenty-First International Conference on Artificial Intelligence and Statistics*. ISSN: 2640-3498. PMLR, pp. 1682–1690. URL: https://proceedings.mlr.press/v84/ge18b.html (visited on 2022).

Gelman, Andrew, Jessica Hwang, and Aki Vehtari (2014). "Understanding predictive information criteria for Bayesian models". en. In: *Statistics and Computing* 24.6, pp. 997–1016. ISSN: 1573-1375. DOI: 10.1007/s11222-013-9416-2. URL: https://doi.org/10.1007/s11222-013-9416-2 (visited on 2022).

Hansen, Anders S et al. (2018). "Robust model-based analysis of single-particle tracking experiments with Spot-On". In: *eLife* 7. Ed. by David Sherratt. Publisher: eLife Sciences Publications, Ltd, e33125. ISSN: 2050-084X. DOI: 10.7554/eLife.33125. URL: https://doi.org/10.7554/eLife.33125 (visited on 2022).

Heltberg, Mathias L et al. (2021). "Physical observables to determine the nature of membrane-less cellular sub-compartments". In: *eLife* 10. Ed. by Agnese Seminara, José D Faraldo-Gómez, and Pierre Ronceray. Publisher: eLife Sciences Publications, Ltd, e69181. ISSN: 2050-084X. DOI: 10.7554/eLife.69181. URL: https://doi.org/10.7554/eLife.69181 (visited on 2022).

Hnisz, Denes et al. (2017). "A Phase Separation Model for Transcriptional Control". en. In: *Cell* 169.1, pp. 13–23. ISSN: 0092-8674. DOI: 10.1016/j.cell.2017.02.007. URL: https://www.sciencedirect.com/science/article/pii/S009286741730185X (visited on 2022).

Hoffman, Matthew D. and Andrew Gelman (2011). "The No-U-Turn Sampler: Adaptively Setting Path Lengths in Hamiltonian Monte Carlo". In: *arXiv:1111.4246 [cs, stat]*. arXiv: 1111.4246.

Klein, Hannah L. et al. (2019). "Guidelines for DNA recombination and repair studies: Cellular assays of DNA repair pathways". en. In: *Microbial Cell* 6.1. Publisher: Shared Science Publishers, pp. 1–64. ISSN: 2311-2638. DOI: 10.15698/mic2019.01.664. URL: http://microbialcell.com/researcharticles/2019a-klein-microbial-cell/,%20http://microbialcell.com/researcharticles/2019a-klein-microbial-cell/ (visited on 2022).

Maillet, L. et al. (1996). "Evidence for silencing compartments within the yeast nucleus: a role for telomere proximity and Sir protein concentration in silencer-mediated repression." en. In: *Genes & Development* 10.14. Company: Cold Spring Harbor Laboratory Press Distributor: Cold Spring Harbor Laboratory Press Institution: Cold Spring Harbor Laboratory Press Label: Cold Spring Harbor Laboratory Press Publisher: Cold Spring Harbor Lab, pp. 1796–1811. ISSN: 0890-9369, 1549-5477. DOI: 10.1101/gad.10.14.1796. URL: http://genesdev.cshlp.org/content/10/14/1796 (visited on 2022).

Manley, Suliana et al. (2008). "High-density mapping of single-molecule trajectories with photoactivated localization microscopy". en. In: *Nature Methods* 5.2. Number: 2 Publisher: Nature Publishing Group, pp. 155–157. ISSN: 1548-7105. DOI: 10.1038/nmeth.1176. URL: https://www.nature.com/articles/nmeth.1176 (visited on 2022).

Marcand, S. et al. (1996). "Silencing of genes at nontelomeric sites in yeast is controlled by sequestration of silencing factors at telomeres by Rap 1 protein". eng. In: *Genes & Development* 10.11, pp. 1297–1309. ISSN: 0890-9369. DOI: 10.1101/gad.10.11.1297.

McElreath, Richard (2020). *Statistical rethinking: a Bayesian course with examples in R and Stan*. 2nd ed. CRC texts in statistical science. Boca Raton: Taylor and Francis, CRC Press. ISBN: 978-0-367-13991-9.

McLachlan, Geoffrey J. and David Peel (2004). *Finite Mixture Models*. en. Google-Books-ID: c2_fAox0DQoC. John Wiley & Sons. ISBN: 978-0-471-65406-3.

Miné-Hattab, Judith et al. (2022). "Single molecule microscopy reveals key physical features of repair foci in living cells". In: *eLife* 10 (), e60577. ISSN: 2050-084X. DOI: 10.7554/eLife.60577. URL: https://www.ncbi.nlm.nih.gov/pmc/articles/PMC7924958/ (visited on 2022).

Oswald, Felix et al. (2014). "Imaging and quantification of trans-membrane protein diffusion in living bacteria". en. In: *Physical Chemistry Chemical Physics* 16.25. Publisher: The Royal Society of Chemistry, pp. 12625–12634. ISSN: 1463-9084. DOI: 10.1039/C4CP00299G. URL: https://pubs.rsc.org/en/content/articlelanding/2014/cp/c4cp00299g (visited on 2022).

Palladino, F. et al. (1993). "SIR3 and SIR4 proteins are required for the positioning and integrity of yeast telomeres". eng. In: *Cell* 75.3, pp. 543–555. ISSN: 0092-8674. DOI: 10.1016/0092-8674(93)90388-7.

Ranjan, Anand et al. (2020). "Live-cell single particle imaging reveals the role of RNA polymerase II in histone H2A.Z eviction". In: *eLife* 9. Ed. by Geeta J Narlikar et al. Publisher: eLife Sciences Publications, Ltd, e55667. ISSN: 2050-084X. DOI: 10.7554/eLife.55667. URL: https://doi.org/10.7554/eLife.55667 (visited on 2022).

Ruault, Myriam et al. (2011). "Clustering heterochromatin: Sir3 promotes telomere clustering independently of silencing in yeast". In: *The Journal of Cell Biology* 192.3, pp. 417–431. ISSN: 0021-9525. DOI: 10.1083/jcb.201008007. URL: https://www.ncbi.nlm.nih.gov/pmc/articles/PMC3101097/ (visited on 2022).

Schober, Heiko et al. (2008). "Controlled exchange of chromosomal arms reveals principles driving telomere interactions in yeast". In: *Genome Research* 18.2, pp. 261–271. ISSN: 1088-9051. DOI: 10.1101/gr.6687808. URL: https://www.ncbi.nlm.nih.gov/pmc/articles/PMC2203624/ (visited on 2022).

Stracy, Mathew and Achillefs N. Kapanidis (2017). "Single-molecule and super-resolution imaging of transcription in living bacteria". en. In: *Methods*. Transcriptional dynamics 120, pp. 103–114. ISSN: 1046-2023. DOI: 10.1016/j.ymeth.2017.04.001. URL: https://www.sciencedirect.com/science/article/pii/S1046202316305011 (visited on 2022).

Swygert, Sarah G. et al. (2018). "SIR proteins create compact heterochromatin fibers". In: *Proceedings of the National Academy of Sciences* 115.49. Publisher: Proceedings of the National Academy

of Sciences, pp. 12447–12452. DOI: 10.1073/pnas.1810647115. URL: https://www.pnas.org/doi/10.1073/pnas.1810647115 (visited on 2022).

Taddei, Angela et al. (2009). "The functional importance of telomere clustering: Global changes in gene expression result from SIR factor dispersion". In: *Genome Research* 19.4, pp. 611–625. ISSN: 1088-9051. DOI: 10.1101/gr.083881.108. URL: https://www.ncbi.nlm.nih.gov/pmc/articles/PMC2665780/ (visited on 2022).

Therizols, Pierre et al. (2010). "Chromosome arm length and nuclear constraints determine the dynamic relationship of yeast subtelomeres". In: *Proceedings of the National Academy of Sciences* 107.5. Publisher: Proceedings of the National Academy of Sciences, pp. 2025–2030. DOI: 10.1073/pnas.0914187107. URL: https://www.pnas.org/doi/abs/10.1073/pnas.0914187107 (visited on 2022).

Watanabe, Sumio (2010). "Asymptotic Equivalence of Bayes Cross Validation and Widely Applicable Information Criterion in Singular Learning Theory". In: *Journal of Machine Learning Research* 11.116, pp. 3571–3594. ISSN: 1533-7928.

Appendix 1

A | APPENDIX FIGURE 1

Here an example of an appendix figure.

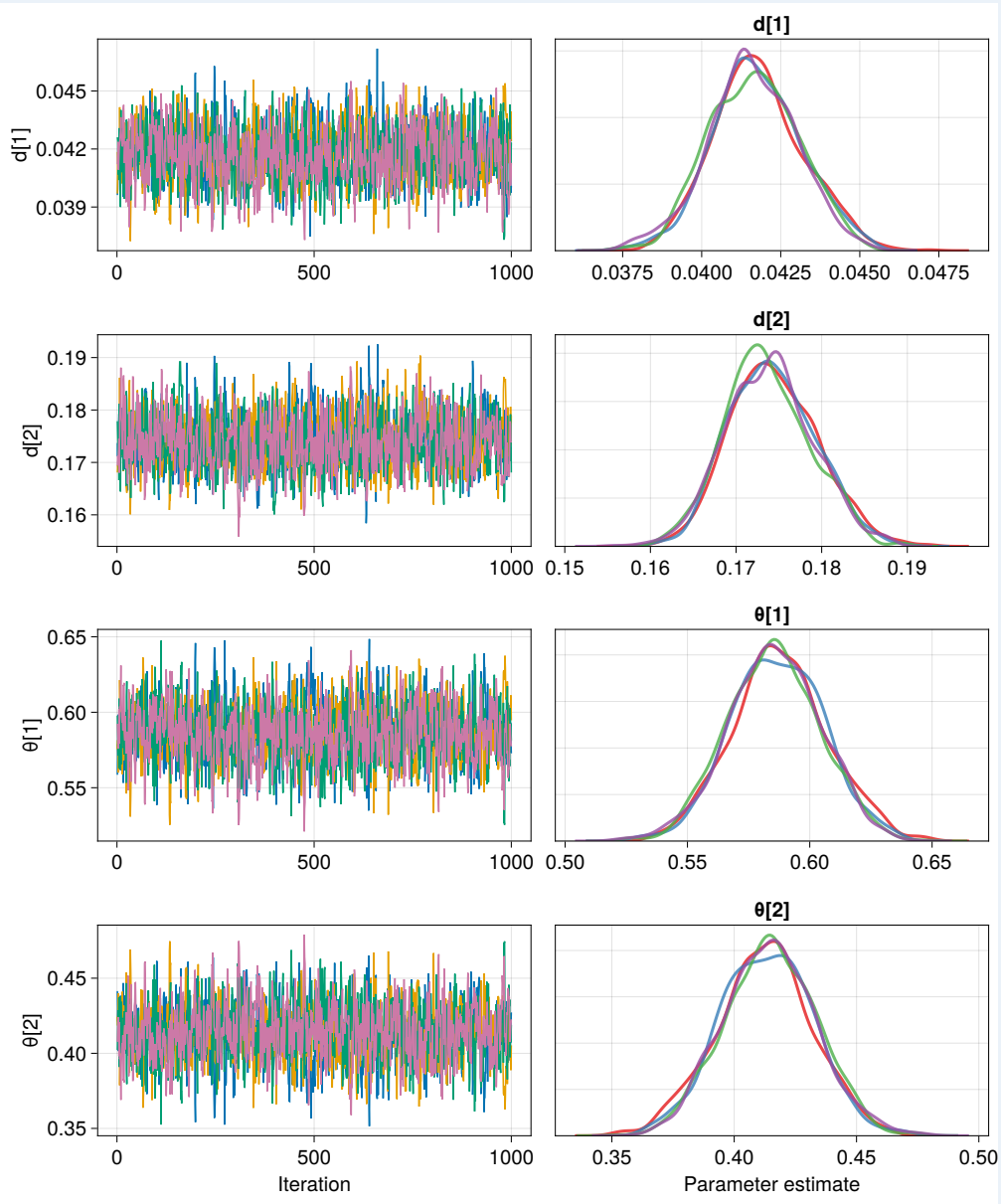

Appendix 1—figure 1. XXX.